

Bayesian multi-proxy reconstruction of early Eocene latitudinal temperature gradients

Kilian Eichenseer¹ and Lewis A. Jones²

¹Department of Earth Sciences, Durham University, South Road, DH1 3LE, Durham, United Kingdom

²Centro de Investigación Mariña, Grupo de Ecoloxía Animal, Departamento de Ecoloxía e Bioloxía Animal, Universidade de Vigo, 36310 Vigo, Spain.

Corresponding author: kilian.eichenseer@durham.ac.uk

Abstract

Accurately reconstructing large-scale ~~palaeoclimate~~ *palaeoclimatic* patterns from sparse local records is critical for understanding the evolution of Earth's climate. Particular challenges arise from the patchiness, uneven spatial distribution, and disparate nature of palaeoclimatic proxy records. Geochemical data typically provide temperature estimates via transfer functions derived from experiments. Similarly, transfer functions based on the climatic requirements of modern taxa exist for some fossil groups, such as pollen assemblages. In contrast, most ecological and lithological data (e.g. coral reefs and evaporites) only convey information on broad climatic requirements. Historically, most large-scale proxy-based reconstructions have used either geochemical or ecological data, but few studies have combined multiple proxy types into a single quantitative reconstruction. Large spatial gaps in existing proxy records have often been bridged by simple averaging, without taking into account the spatial distribution of samples, leading to biased temperature reconstructions. Here, we present a Bayesian hierarchical model to integrate ecological data with established geochemical proxies into a unified quantitative framework, bridging gaps in the latitudinal coverage of proxy data. We apply this approach to the early Eocene climatic optimum (EECO), the interval with the warmest sustained temperatures of the Cenozoic. Assuming the conservation of thermal tolerances of modern coral reefs and mangrove taxa, we establish broad sea surface temperature ranges for EECO coral reef and mangrove sites. We integrate these temperature estimates with the EECO geochemical shallow marine proxy record to model the latitudinal sea surface temperature gradient and global average temperatures of the EECO. Our results confirm the presence of a flattened latitudinal temperature gradient and unusually high polar temperatures during the EECO, which is supported by high-latitude ecological

Style Definition: Footnote Text: Font: 11 pt, Font color: Text 1, Right

32 data. We show that integrating multiple types of proxy data, and adequate prior information, has the
33 potential to ~~substantially reduce uncertainty in palaeoclimate~~ enhance quantitative palaeoclimatic
34 reconstructions, ~~allowing for unbiased~~ improving temperature estimates from ~~sparse data~~ datasets with
35 limited spatial sampling.

36 **Keywords**

37 Palaeoclimate, latitudinal temperature gradients, temperature proxies, Eocene, ~~spatial~~ sampling bias,
38 Bayesian

39 **Introduction**

40 Understanding the long-term evolution of Earth's climate system and contextualising ~~current~~ contemporary
41 global warming relies on accurate reconstructions of past climates (Royer et al., 2004; Burke et al., 2018;
42 Tierney et al., 2020). Recent advances in the synthesis of ~~palaeoclimate~~ palaeoclimatic data (e.g. Veizer and
43 Prokoph, 2015; Hollis et al., 2019; Song et al., 2019; Grossman and Joachimski, 2022; Judd et al., 2022)
44 are offering unprecedented insights into the complex and dynamic nature of the Earth's climate system, yet
45 a fundamental challenge remains: the proxy record of past climates is spatially incomplete and afflicted by
46 imperfect preservation and uneven sampling (Judd et al., 2020; Jones and Eichenseer, 2022; Judd et al.,
47 2022).

48 ~~Whilst~~ Acknowledging the assumptions and limitations inherent in geochemical temperature proxies, such
49 as experimentally derived calibrations, influences from seasonality, dissolution effects and differential
50 preservation (e.g. Tierney et al., 2017 proxy data), can provide enable robust estimates of palaeotemperature
51 at local scales. However, recent work has demonstrated that spatial biases in the geochemical proxy record
52 can lead to spurious estimates of regional (e.g. latitudinal temperature gradients) and global temperatures
53 (Judd et al., 2020; Jones and Eichenseer, 2022). Principally, this can be driven by two factors: (1) missing
54 data for some regions (e.g. no high-latitude data); or (2) overrepresentation of other regions (e.g. a high
55 proportion of samples from tropical areas). The latter can be addressed through the down-sampling of data
56 or restricting analyses to specific regions (e.g. Song et al., 2019). However, in order to robustly infer
57 regional or global-scale patterns from an incomplete record, spatial gaps must ultimately be bridged. One
58 common approach, which requires no additional computation, is the spatial visualisation of proxy-derived
59 temperatures against latitude, showing broad latitudinal temperature trends (e.g. Hollis et al., 2019; Vickers
60 et al., 2021). Interpolation is also sometimes used to bridge spatial gaps in ~~palaeoclimate~~ palaeoclimatic data
61 (e.g. Taylor et al., 2004), taking advantage of the autoregressive nature of climatic data: much of the

62 information on the climate of any given location is contained in the climate data of nearby locations
63 (Reynolds and Smith, 1994). Adding to this, some proxy-based reconstructions use statistical modelling to
64 infer palaeoclimatic patterns. For example, polynomial regression (Bijl et al., 2009) and cosine functions
65 (Inglis et al., 2020) have been used to reconstruct latitudinal temperature gradients, and 2D-reconstructions
66 of surface temperatures have been created with Gaussian process regression (Inglis et al., 2020). These
67 approaches work well for interpolating relatively densely-sampled data, but the absence of constraints on
68 the modelled parameters means that such models can produce unrealistic temperature estimates when
69 extrapolating from sparse data. Statistical modelling in a Bayesian framework can help overcome this
70 problem by requiring the explicit specification of priors for the model parameters, which can be used to
71 express physical constraints (Chandra et al., 2021).

72 Spatial gaps in the ~~palaeoclimate~~palaeoclimatic record can also be addressed through the integration of
73 additional data. For example, lithological and fossil data can be used to infer past climatic conditions based
74 on analogous modern sediments (Chandra et al., 2021), or based on the premise that the climatic
75 requirements of ancient taxa, biological traits, or ecological communities were similar to those of their
76 nearest modern relatives (Peppe et al., 2011; Royer, 2012; Salonen et al., 2019). Despite this potential, the
77 integration of geochemical proxy data with other sources of information (e.g. ecological data) has rarely
78 been realised in a rigorous, quantitative framework (Burgener et al., 2023).

79 Here, we present a novel Bayesian hierarchical model (e.g. Gelman et al., 2013; McElreath, 2018) that
80 combines quantitative proxies and ecological constraints into a fully quantitative model of the latitudinal
81 gradient of sea surface temperatures, bridging spatial gaps in sparsely sampled ~~climate data~~palaeoclimatic
82 data. The Bayesian approach offers a powerful framework for integrating various sources of uncertainty
83 and modelling complex hierarchical relationships, and is increasingly used in palaeoclimatic
84 reconstructions (e.g. Weitzel et al., 2019; Yang and Bowen, 2022; Burgener et al., 2023). This model
85 expands upon existing, spatially explicit palaeoclimatic reconstructions by allowing for the integration of
86 (1) prior information based on physical principles and the observed modern sea surface temperature
87 distribution, and of (2) geochemical and ecological ~~climate~~palaeoclimatic proxies in a common,
88 quantitative framework. We ~~use~~choose a generalised logistic function to accurately infer the shape of the
89 temperature gradient despite a patchy latitudinal coverage, ~~and~~. This choice is motivated by the flexibility
90 and ability of this function to approximate a variety of nonlinear patterns in the underlying temperaiture
91 gradients that other parametric approaches, such as lower order polynomials (e.g. Bijl et al., 2009; Keating-
92 Bitonti et al., 2011), lack. We test the robustness of this method using down-sampled, simulated latitudinal
93 temperature gradients.

94 We apply this model to the record of the early Eocene climatic optimum (EECO), combining a compilation
 95 of geochemical proxies (Hollis et al., 2019), mangrove communities (Popescu et al., 2021), and coral reefs
 96 (Zamagni et al., 2012), ~~using~~. We use a nearest-living-relative approach (e.g. Greenwood et al., 2017) to
 97 establish broad temperature ranges for the ecological data. We choose the EECO to demonstrate the
 98 application of the model due to its significance as the interval with the warmest sustained temperatures of
 99 the Cenozoic (Pross et al., 2012), rendering it a potential analogue for extreme climate warming scenarios
 100 (Burke et al., 2018). Our integrative approach allows us to shed new light on the long-standing dispute on
 101 the steepness of the early Eocene temperature gradient (Table 1; Sloan and Barron, 1990; Markwick, 1994;
 102 Huber and Caballero, 2011; Tierney et al., 2017; Inglis et al., 2020).

103 Table 1: Inferred latitudinal sea surface temperature (SST) gradients for the early Eocene (EE) or the EECO,
 104 as shown in earlier, proxy-based studies. The gradient values denote the SST difference between the equator
 105 and the polar circle, or other types of gradients. For comparison, a gradient derived from an atmosphere-
 106 ocean general circulation model (GCM) ensemble ~~is~~, and a range of gradients from a model intercomparison
 107 project, are also shown.

Source	Time	Gradient (°C)	Type of gradient	Model	Proxy system
Bijl et al. (2009)	EE	7	equator - polar circle	2 nd order polynomial	TEX ₈₆ , UK ₃₇ ^{K'}
Keating-Bitoni et al. (2011)	EECO	13	equator - polar circle	2 nd order polynomial	TEX ₈₆ , MBT/CBT, Δ ₄₇ , Mg/Ca, δ ¹⁸ O
Tierney et al. (2017)	EE	12	equator - polar circle	Gaussian function	TEX ₈₆
Cramwinckel et al. (2018)	EECO	21 (±1)	equator - deep water	-	TEX ₈₆ , Δ ₄₇ , Mg/Ca, δ ¹⁸ O, deepwater δ ¹⁸ O
Evans et al. (2018)	EE	20 (±3)	tropics - deep water	-	Δ ₄₇ , deepwater Mg/Ca
Pross et al. (2012), as shown in Tierney et al. (2017)	EE	26	equator - polar circle	climate model ensemble (GCM)	none (GCM simulations)
<u>Lunt et al. (2021)</u>	<u>EECO</u>	<u>18–26</u>	<u>tropics - high latitude</u>	<u>DeepMIP climate models</u>	<u>none (GCM simulations)</u>

108 **Materials & Methods**

109 **Geochemical data**

110 Geochemical ~~climate~~climatic proxy data were extracted from a latest Paleocene and early Eocene
111 compilation (Hollis et al., 2019). This compilation provides sea surface temperature data on four different
112 geochemical proxies for reconstructing seawater temperature: $\delta^{18}\text{O}$, Δ_{47} , Mg/Ca and TEX_{86} . For our
113 analyses, this dataset was restricted to the EECO (defined as 53.8—49.1 Ma) and samples originating
114 from near the ~~continental shelf~~ocean surface or mixed layer. Consequently, samples labelled as
115 “thermocline”, or “sub-thermocline”, were excluded. Recrystallised $\delta^{18}\text{O}$ samples were also excluded as
116 secondary diagenetic calcite precipitated after deposition can bias isotope measurements and offset
117 temperature values (Schrag, 1999). This filtering resulted in most $\delta^{18}\text{O}$ samples being excluded from the
118 dataset (retaining 8 out of 152). After data filtering, 308 geochemical proxy samples from 23 locations
119 remained. (Fig. 1). For a detailed description of each proxy see Hollis et al. (2019).

120 **Ecological data**

121 **Coral reefs.** Today, shallow warm-water coral reefs are limited to tropical and subtropical latitudes ($\sim 34^\circ \text{N}$
122 —32 $^\circ \text{S}$), with minimum sea surface temperature tolerances ($\sim 18^\circ \text{C}$) being the primary constraint on this
123 distribution (Johannes et al., 1983; Kleypas et al., 1999; Yamano et al., 2001). As coral reefs reside at the
124 upper thermal limit of the oceans today, their maximum sea surface temperature tolerance is less well-
125 constrained, with some studies suggesting up to 35.6°C in the geological past (Jones et al., 2022).
126 Nevertheless, coral reefs have frequently been recognised as tracers of past (sub-)tropical conditions
127 (Ziegler et al., 1984; Kiessling, 2001). During the Eocene, coral communities and reefs expanded across
128 tropical and temperate latitudes, with communities found up to palaeolatitudes of 43°N (Zamagni et al.,
129 2012). Using a compilation of Paleocene—early Eocene coral reefs and community localities (Zamagni
130 et al., 2012), we generated quantitative sea surface temperature estimates for the EECO. To do so, we
131 extracted localities from the compilation that are inferred to be Ilerdian (early Eocene) coral reefs, and that
132 could be confidently assigned to the EECO. We excluded coral knobs and coral-bearing mounds which
133 might have broader climatic limits than warm-water coral reef ecosystems. This filtering resulted in four
134 unique coral reef localities remaining for the EECO, all of which conform to the modern latitudinal range
135 of coral reefs ($< 34^\circ \text{N}$). Subsequently, we used statistically derived temperature limits (minimum = 21°C ,
136 average = 27.6°C , maximum = 29.5°C) from the published literature (Kleypas et al., 1999) to define a
137 normal probability distribution of potential temperature values for coral reef localities. This normal
138 probability distribution was defined with a mean of 27.6°C and a standard deviation of 2.125, placing
139 97.5% $^\circ \text{C}$, which places the minimum (21°C) at the lower end of the probability 95% highest density above

140 ~~the minimum~~ interval of that distribution. As the distribution of modern corals is skewed towards warmer
141 temperatures, this approach results in 16.5% of the probability being placed on temperatures > 29.5°C,
142 allowing for the possibility that Eocene coral reefs were adapted to warmer conditions than present-day
143 coral reefs.

144 **Mangroves.** Mangroves are distributed throughout the tropics and subtropics today. While factors besides
145 sea surface temperatures (SST) influence the distribution of mangroves, empirical lower temperature limits
146 have been established for the genera *Avicennia* (15.6°C) and *Rhizophora* (20.7°C) (Quisthoudt et al., 2012).
147 Both *Avicennia* and members of the Rhizophoraceae family were widespread and co-occurred across
148 tropical and temperate latitudes in the early Eocene. Only *Avicennia*, however, occurred at polar latitudes
149 (Suan et al., 2017; Popescu et al., 2021). Assuming that Eocene members of these mangrove taxa conform
150 to similar climatic requirements as their modern relatives, the presence and absence of *Avicennia* and
151 Rhizophoraceae pollen can be used as a palaeotemperature indicator. For this analysis, published mangrove
152 occurrence data were taken from Popescu et al. (2021), and converted to quantitative temperature estimates.
153 From this data, we identify two types of pollen assemblages which we ascribe different temperature
154 distributions:

- 155 1) *Avicennia*-only assemblages ($n = 2$): the absence of Rhizophoraceae is indicative of temperatures
156 ~~being~~ between 15.6°C (lower temperature limit of *Avicennia*) and 20.7°C (lower temperature
157 limit of *Rhizophora*). However, a value of 22.5°C is ~~ascribed~~ assumed as the upper temperature
158 limit here as *Rhizophora* is rare below this temperature. We define the *Avicennia*-only
159 temperature distribution as a normal distribution with a mean of 19.05°C and a standard deviation
160 of 1.725°C, resulting in 95% of the probability density being placed within the temperature limits.
- 161 2) *Avicennia* and Rhizophoraceae assemblages ($n = 5$): the presence of both groups suggests that
162 the locality should have a minimum temperature of 20.7°C (lower temperature limit of
163 *Rhizophora*). As the upper thermal limits of *Avicennia* and *Rhizophora* are not well established
164 in Quisthoudt et al. (2012), we assign the same maximum temperature limits (29.5°C) as coral
165 reef localities, because mangroves are also widely distributed throughout tropical regions.
166 Consequently, we define the temperature distribution for this locality as a normal distribution
167 with a mean of 25.1°C and a standard deviation of 2.2°C, with 95% probability density within the
168 temperature limits.



Figure 1: Palaeogeographic distribution of the geochemical and ecological data compilation used in this study. Map is presented in the Robinson projection (ESRI:54030).

169 **Palaeogeographic reconstruction**

170 The palaeogeographic distribution of geochemical and ecological data was reconstructed using the Merdith
 171 et al. (2021) [plate rotation model](#) [Global Plate Model](#) via the palaeoverse R package (version 1.2.0, Jones et

172 al., 2023). The midpoint age of the EECO (51.2 Ma), along with the present-day coordinates of geochemical
 173 and ecological data, were used for palaeogeographic reconstruction.

174 **Bayesian framework**

175 **Model structure.** We model the mean temperature (μ) at location j as a function of absolute latitude
 176 ($abs(l)$) with a logistic regression (also known as “growth curve” or “Richard’s curve”) of the form:

$$177 \quad \mu_j \sim N(v_j, \sigma), \quad (1)$$

$$178 \quad v_j = A + \frac{K-A}{e^{\frac{B(abs(l_j)-M)}{1+e^{B(abs(l_j)-M)}})}}, \quad j = 1, \dots, n, \quad (2)$$

179 where A and K denote the lower and upper asymptote, respectively, M specifies the latitude of maximal
 180 growth, i.e. the latitude around which temperature falls most steeply with latitude, B denotes the growth
 181 rate, σ denotes the residual standard deviation, and n denotes the number of locations.

182 We use this generalised logistic function because it can follow the equatorial and polar asymptotes observed
 183 in the modern, latitudinal SST gradient, but can also accommodate a variety of other shapes, while
 184 consisting of only four shape parameters. This flexibility is primarily achieved by shifting the location of
 185 the curve along the latitudinal axis by varying M , and by altering the steepness of the curve by varying B .
 186 For example, one limb of a second-order polynomial as in Bijl et al. (2009) can be approximated by
 187 increasing M towards high latitudes, and decreasing B to reduce the steepness of the curve. The model is
 188 designed for modelling the average gradient across both hemispheres, but can also be applied to individual
 189 hemispheres, to assess hemispherical differences (see Fig. S4).

190 We infer μ_j from m individual temperature observations $t_{i=1..m}$, derived from geochemical data, at
 191 location j as

$$192 \quad t_{i,j} \sim N(\mu_j, \sigma_j), \quad i = 1, \dots, m, \quad (3)$$

193 where m is the number of observations at each location, and σ_j is the estimated standard deviation of the
 194 temperatures at location j .

195 Similarly, μ_j is inferred for locations with ecological proxies from the associated normal temperature
 196 distributions with a given mean and standard deviation, $t_{\mu,j}$ and $t_{\sigma,j}$, as

$$197 \quad t_{\mu,j} \sim N(\mu_j, t_{\sigma,j}). \quad (4)$$

198 This structure implies that μ_j is not fixed at the mean proxy temperature at location j , but is drawn towards
 199 the overall logistic regression curve, i.e. towards v_j . The pull towards v_j tends to be strong when m is low,
 200 when the observations $t_{i=1,\dots,m,j}$ are scattered, i.e. σ_j is high, and/or when the overall standard deviation σ
 201 is low. In practice, this has the desirable consequence that locations with few observations and large
 202 temperature differences between observations have less influence on the overall regression than well-
 203 sampled locations with consistent reconstructed temperatures.

204 [We show an expanded model that includes uncertainties on individual temperature observations in the](#)
 205 [Supplementary Material \(Fig. S5\).](#)

206 **Priors.** In a Bayesian framework, priors need to be placed on the unknown parameters of a model. We
 207 placed weakly informative, conjugate inverse-gamma priors on σ and $\sigma_{j=1,\dots,n}$:

$$208 \quad \sigma \sim \sqrt{\text{Inv-Gamma}\left(\alpha + \frac{n}{2}, \beta + 0.5 \times (\mu_j - v_j)\right)}, \quad j = 1, \dots, n, \quad (5)$$

$$209 \quad \sigma_j \sim \sqrt{\text{Inv-Gamma}\left(\alpha + \frac{m}{2}, \beta + 0.5 \times (t_{i,j} - \mu_j)\right)}, \quad i = 1, \dots, m, \quad j = 1, \dots, n. \quad (6)$$

210 We set $\alpha = \beta = 1$, allowing these priors to be quickly overwhelmed by the data as n and m increase, as
 211 we have little *a priori* knowledge of these parameters.

212 In contrast, we put informative priors on the regression coefficients A , K , M and B , based on physical
 213 principles, and loosely based on the modern climate system:

214 **A.** Predicted seawater surface temperatures are not allowed to be $\ll -2^{\circ}\text{C}$, the freezing point of sea
 215 water. The highest prior density of A is placed around 0°C , and it slowly tapers off towards higher
 216 temperatures. This shape is achieved by placing a skew-normal prior on the lower asymptote, specified as

$$217 \quad A \sim \text{SN}(\xi = -3.0, \omega = 12, \alpha_{\text{SN}} = 30), \quad (7)$$

218 where ξ , ω , and α_{SN} are the location, scale and shape parameters.

219 **K.** Input of solar energy decreases from the tropics to the poles. Hence, the latitudinal temperature gradient
 220 is broadly negative, i.e. temperature decreases with absolute latitude. This is achieved by setting $K \geq A$.
 221 The prior on the upper asymptote K is a truncated normal distribution with the mean set to K of the modern
 222 SST gradient, with a broad standard deviation:

223
$$K \sim TN(\mu_{TN} = 28, \sigma_{TN} = 15, \alpha_{TN} = A, \beta_{TN} = \infty) \quad (8)$$

224 The distribution is truncated to the left at $\alpha_{TN} = A$, but not truncated to the right (β_{TN}).

225 **M.** A uniform prior is placed on the latitude of greatest steepness of the gradient, allowing it to be steepest
226 anywhere between latitudes 0° and 90° absolute latitude, as this parameter may vary greatly depending on
227 the climate state:

228
$$M \sim Uniform(0,90) \quad (9)$$

229 **B.** The steepness or growth rate B of the gradient is constrained to be ≥ 0 and to not be exceedingly high,
230 as oceanic and atmospheric heat transfer is bound to limit very abrupt SST changes across latitudes on a
231 global scale. A gamma-distributed prior of the form

232
$$B \sim Gamma(\alpha_G = 4.3, \beta_G = 30) \quad (10)$$

233 was placed on B . The shape and rate parameters α_G and β_G were chosen such that the highest prior density
234 is at B of the modern SST gradient, 0.11. We informed the prior distribution on B based on a provisional
235 model run with the modern SST data.

236 **Model validation**

237 To test whether our logistic regression model can adequately describe different latitudinal temperature
238 gradients at various sample sizes, we ~~generated four~~ focused the empirical, modern gradient, representative of
239 an icehouse climate, and generated three idealised gradients that emulate potential climatic states
240 throughout Earth's geological history: extreme icehouse, icehouse-~~(modern)~~, greenhouse, and extreme
241 greenhouse (Frakes et al., 1992). The idealised gradients serve to test whether our model setup is able to
242 infer gradients that are strongly different from the modern from a varying number of samples.

243 We ~~then created test data from these gradients as follows: We~~ randomly sampled ~~(4,000)1000~~ iterations)
244 ~~these gradients using increasing latitudes at~~ sample sizes ~~(of 5, 10, and 20)~~ and reconstructed the latitudinal,
245 with the probability of a latitude being sampled scaling with the decreasing surface area towards higher
246 latitudes, i.e. lower latitudes are sampled more frequently. For the largest sample size ($n = 34$), we used the
247 latitudes of the EECO data set of this study in all iterations. For each latitude, we took the location mean
248 temperature gradient using our model for each of these sample sizes and gradient types. Using the same
249 idealised gradients, we also tested whether our model could accurately reconstruct latitudinal temperature
250 gradients using the palaeogeographic from the gradients, adding random noise from a normal distribution
251 of Eocene samples ($n = 34$), providing an empirical, exemplary distribution that captures both limited
252 sample size and skewed geographic origins of samples, with a standard deviation of 3.8, which corresponds

253 to the average uncertainty associated with [the EECO geochemical proxy data](#) (Hollis et al. 2019). [With that,](#)
254 [we aim to simulate randomly distributed errors in the proxy data, which could arise from miscalibrations,](#)
255 [measurement errors, seasonal effects, ect. We acknowledge that this approach cannot quantify the potential](#)
256 [impact of systematic offsets that may bias all proxy data in the same direction, nor do we know whether a](#)
257 [standard deviation of 3.8 is the actual average magnitude of uncertainty that the proxy compilation is](#)
258 [afflicted with.](#)

259 To evaluate how well the model performed in reconstructing the idealised gradients from limited sampling,
260 we calculated the coefficient of determination (R^2) for Bayesian regression models (Gelman et al., 2019).
261 For every iteration from the posterior, we intercepted the modelled and the idealised gradient in intervals
262 of 1° latitude and calculated the R^2 based on these values. We report the median, and 95% credible intervals
263 (CI) of the resulting R^2 values. Here and in all other instances, the 95% CI refer to the interval between the
264 2.5% point and the 97.5% point of the samples or sampled posterior distribution.

265 To test whether our model can accurately depict the shape of the modern sea surface temperature gradient,
266 and to facilitate comparison with the Eocene gradient, we applied our model to [mean](#) annual sea surface
267 ~~mean~~-temperatures from Bio-Oracle (Assis et al., 2018), aggregated to a [spatial grid resolution of](#) $1^\circ \times 1^\circ$
268 ~~rafter~~ ($n = 46,131$). The R^2 for the modern gradient was calculated as above (Gelman et al., 2019),
269 comparing the modelled gradient and the empirical temperature averages in 1° latitude bins. Only the
270 medians are reported for the modern gradient, as the 95% credible intervals are extremely narrow due to
271 the high precision of the posterior estimates.

272 To reconstruct the idealised gradients and the modern gradient, we used a simplified, non-hierarchical
273 version of our model, as every location is associated with only one temperature value, making the
274 hierarchical structure superfluous. To achieve this, we substituted temperature (t_j) for μ_j in Equation 1 and
275 Equation 5.

276 **Parameter estimation**

277 We estimated the posterior distributions of the model parameters using a Markov chain Monte Carlo
278 (MCMC) algorithm, written in R. Specifically, we sampled the unknown parameters A , K , M and B with
279 Metropolis-Hastings, and used Gibbs sampling to estimate all other unknown parameters (see Gilks et al.,
280 1995; Gelman et al., 2013). Posterior inference on the modern gradient is based on four chains with 60,000
281 iterations each, 10,000 of which were discarded as burn-in. Every ~~10th~~ 10^{th} iteration was retained, resulting
282 in a total of 20,000 iterations with low autocorrelation. The re-sampled, simulated gradients and the re-
283 sampled, modern gradient were modelled in one chain with 10,000 iterations for each of the 1,000 random

Formatted: Body Text

284 samples. 5,000 iterations each were discarded as burn-in, and every ~~25th~~^{25th} iteration was kept, resulting
285 in a total of 200,000 iterations across all 1,000 model runs. For the Eocene model, we ran four chains with
286 600,000 iterations each, discarding 100,000 as burn-in and keeping every ~~100th~~^{100th} iteration, as the
287 hierarchical model structure results in higher autocorrelation of the chains. The Eocene posterior inference
288 is thus based on a total of 20,000 iterations with low autocorrelation (effective multivariate sample size for
289 A , K , M and B is $> 18,000$). Trace plots of the MCMC chains indicate convergence and good mixing of the
290 chains (Fig. S1).

291 **Processing of model results**

292 ~~modelled~~Modelled sea surface temperature estimates were generated with Equation 2, calculating the sea
293 surface temperatures at any latitude with the parameter estimates of each iteration from the posterior
294 samples. The median and 95% CI of temperatures ~~where~~were then taken from all temperature estimates
295 obtained at the latitudes of interest.

296 The latitudinal gradient ~~is~~was calculated as the difference between the modelled temperature at the equator
297 (0° latitude) and at the poles (90° absolute latitude). To facilitate comparison with earlier estimates, we also
298 ~~calculate~~calculated the gradient with the temperature at the polar circle (66.6° absolute latitude) being used
299 instead of the temperature at the poles. ~~Given the sigmoidal shape of the modern as well as the Eocene~~
300 ~~gradient (see Fig. 4), these results are broadly comparable to a gradient inferred from the zonal average of~~
301 ~~equatorial and high latitude temperatures, as has been done in some earlier studies (Evans et al., 2018).~~

302 Differences between Eocene and modern temperatures at a certain latitude were calculated by randomly
303 pairing all iterations of the posterior from the Eocene and modern temperature gradient model, calculating
304 the Eocene and modern temperature using the respective iterations, taking the difference, and then
305 calculating the median (95% CI) from all pairs of iterations.

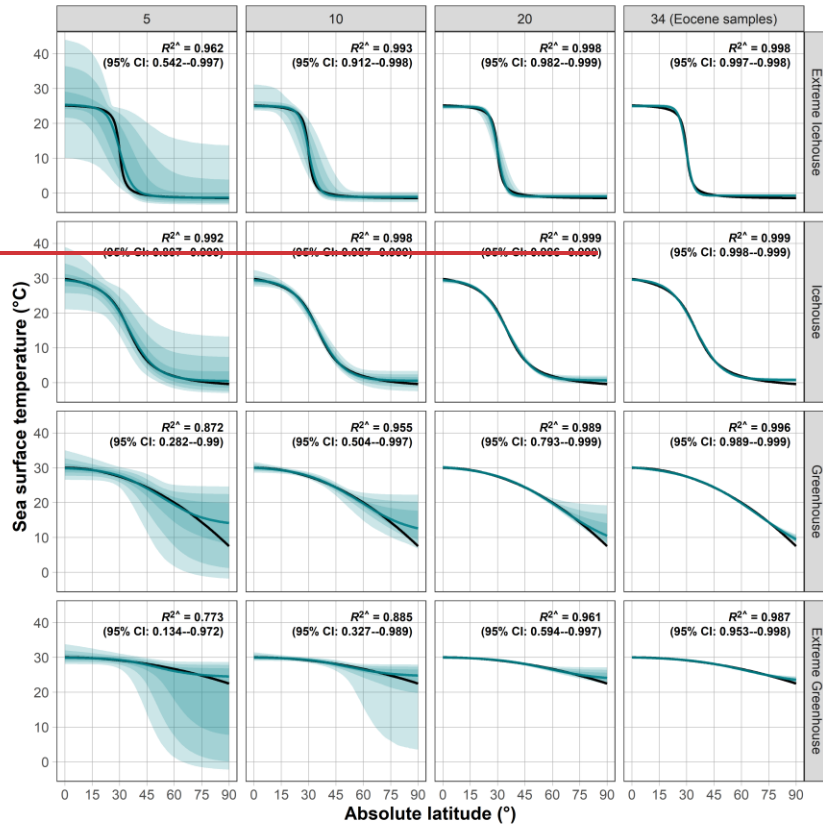
306 Global average temperatures with 95% credible intervals were calculated by taking the weighted mean of
307 the median (95% CI) of temperature estimates in 1° latitudinal bins. The weights were set to the proportion
308 of global surface area in each latitudinal bin, i.e. decreasing with increasing latitude as:

$$309 \quad weights = \sin(\alpha_{1,i}) - \sin(\alpha_{2,i}), \quad (11)$$

310 where α_1 is the upper, and α_2 is the lower latitudinal boundary of bin i , i.e. we approximated the shape of
311 the globe as a spheroid.

312 **Results**

313 **Model validation**



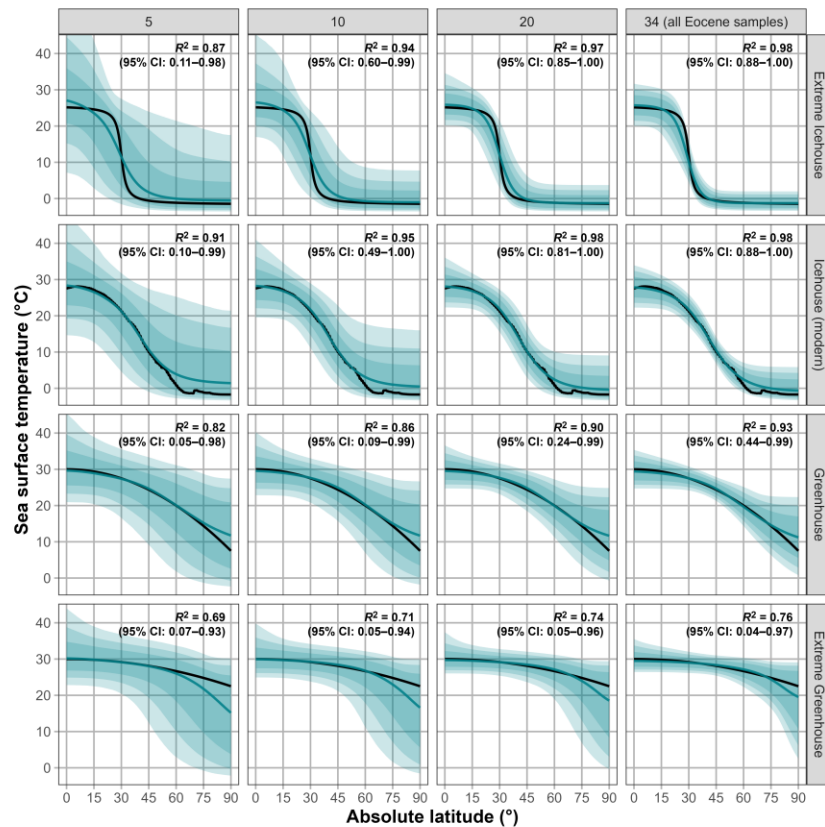


Figure 2: Model reconstructions of simulated latitudinal temperature gradients at various sample sizes. Each column depicts a different reconstruction for given sample sizes: 5, 10, 20 (randomly sampled latitudes), and 34 (latitudes of EECO samples). Each row depicts a different ~~simulated~~ latitudinal temperature gradient that represents idealised ~~or observed~~ climatic states: ~~idealised~~ extreme icehouse, ~~icehouse~~, greenhouse, and extreme greenhouse: ~~gradients, and the modern gradient, which represents an icehouse state~~. The black line illustrates the ~~simulated~~ original gradient. The blue line depicts the reconstructed gradient represented by the median sea surface temperature value estimated from 1,000 model runs with different random samples. ~~To generate the random samples, different random noise from a normal distribution with a standard deviation of 3.8°C was added to each temperature~~. The blue shadings depict the 90%, 95%, and 99% credible intervals. Bold black text within each panel depicts the coefficient of determination (R^2) for estimating goodness of fit between the simulated and modelled gradient. The median (50%) R^2 value along with the 95% credible intervals from all model runs are shown. Each gradient is depicted in absolute latitude.

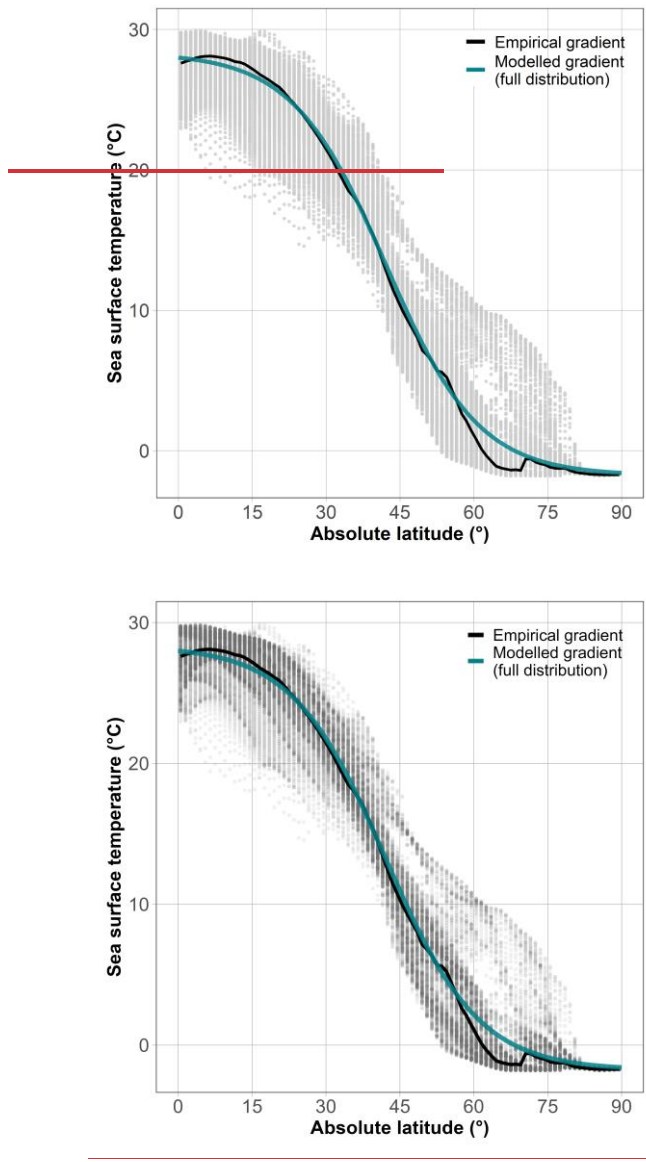


Figure 3: Present-day latitudinal temperature gradient. The present-day empirical latitudinal temperature gradient (median sea surface temperature) is depicted as a black line, and the gradient estimated by the Bayesian model is shown in turquoise ($R^2 = 0.97, N = 42,896$). Grey points depict the individual cell values of the Bio-ORACLE grid of mean sea surface temperatures, which were used

to infer the empirical and the modelled gradient. Higher opacity of points indicates higher density of data (multiple overlapping points).

Our Bayesian model is able to accurately model a range of idealised temperature gradients, ranging from extreme icehouse to ‘super greenhouse’ scenarios (Fig. 2). Random latitudinal sampling results in highly accurate reconstructions for most random samples at sample sizes as low as of 10 and 20 for the icehouse scenarios (95% CI median of $R^2 > 0.9$). Greenhouse scenarios require additional samples perform somewhat worse due to accurately predict the increased uncertainty at high-latitude temperatures. This is because in the absence of high-latitude samples, the modelled gradient is heavily influenced by the priors, which we based on the modern, the only empirically known latitudinal temperature gradient. Latitudes (median of $R^2 > 0.7$ at sample sizes 10 and 20). A sampling distribution resembling that of the early Eocene data set dataset used in this study allows for a highly-accurate reconstruction of even all scenarios, although the R^2 is still relatively low in the extreme greenhouse scenario (95% CI of $R^2 > 0.95$), as a perfectly flat gradient, predicted by the model, would result in an R^2 of 0, despite the original gradient being very flat. This also explains the low lower bounds of the 95% credible intervals in the greenhouse scenarios.

The average, modern temperature gradient can be closely approximated with our model when using the full modern SST dataset (Fig. 3); almost all of the variation in the empirical median temperatures in bins of 1° absolute latitude (black line) is explained by the modelled gradient ($R^2 = 0.997$, 99.7%). The empirical gradient spans 29.3°C from the equator to the poles, the modelled gradient is only slightly higher at 29.6°C . The modern, global mean temperature (GMST) based on our modelled, median gradient is 17.6°C , very similar which is nearly equal to the GMST derived from the empirical median gradient (17.5°C).

EEO reconstruction

The modelled Eocene temperature gradient reconstructed with our Bayesian model is starkly different from the modern (Fig. 4). Modelled, median equatorial temperatures are $4.2, 2^\circ\text{C}$ (95% CI: -0.2 – 8.3)– 8.5°C) higher for the EEO, and polar temperatures are 25.0 (17.0 – 29.1)– 18.9°C (5.3 – 28.9°C) higher. This results in a flattened latitudinal temperature gradient of 9.0 (13.3°C (3.9 – 25.2 , 5 – 17.8)– $^\circ\text{C}$) for the EEO, as opposed to 29.6°C for the modern. To facilitate the comparison with latitudinal gradients reported in the literature, which sometimes do not report temperatures at very high latitudes, we report also the EEO gradient between the equator and the modern-day polar circle (66.6° latitude), which is slightly markedly lower at 75.8 (2.2 – 13.7)– $^\circ\text{C}$, (0.5 – 12.8°C).

The high variability of EEO palaeotemperature proxies, particularly in the mid-latitudes, and the scarcity of high-latitude data, result in substantial uncertainties in the modelled temperature gradient. This is reflected in the residual standard deviation (σ) of the EEO gradient— 4.9°C (3.8 – 9 – 6.5)– $^\circ\text{C}$ —which

345 is more than double the σ for the modern gradient, 2.2°C . This ~~signifies that the early Eocene data does not~~
346 ~~fit as well to the logistic latitudinal gradient model, which can also be seen from~~ ~~is illustrated by~~ the drastic
347 departure of some of the proxy data from the gradient estimates (Fig. 4).

348 The early Eocene GMST is estimated at 28.73°C (26.7 — 30.3°C), 10.7°C , 11.1°C higher than the
349 modern. A model run excluding the ecological proxies increases the GMST by 1.67°C (-1.8 — 4.8° —
350 5.0°C). The median ~~latitudinal gradient is similar~~ ~~modelled temperature is higher near the equator and in~~
351 ~~high latitudes~~ when excluding the ecological proxies, with a ~~flattened~~ median gradient of 10.9 — 2°C , but with
352 a ~~20% wider 95% CI~~ $^{\circ}\text{C}$ (Fig. S2). ~~This indicates that the~~ ~~In contrast, including ecological proxies, but~~
353 ~~widening the uncertainty around the low-latitude~~ ecological proxy data ~~are broadly in agreement with the~~
354 ~~geochemical proxies, while providing additional constraints on the shape of~~ ~~does not significantly change~~
355 ~~the early Eocene temperature resulting gradient.~~ (Fig. S3).

356 Due to the limited spatial coverage of the early Eocene proxy record, and due to the added model complexity
357 of simultaneously estimating a model across both hemispheres, we pooled the proxy data across both
358 hemispheres. Applying the model separately within each hemisphere results in substantial differences in
359 hemispherical, average temperatures, with the Southern Hemisphere being warmer by 6.5 (3.5 — 1°C
360 (2.9 — 4° — 9.2°C). The inferred latitudinal gradient is somewhat steeper in the Northern Hemisphere (steeper
361 by 4 — 8°C , although the 95% CI ~~of that difference~~ spans -6.6 — 18.0 — 14.35°C), but the large uncertainties
362 associated with both gradients, and the lack of polar proxy data in the Southern Hemisphere preclude a
363 more precise statement (see Fig. S3S4).

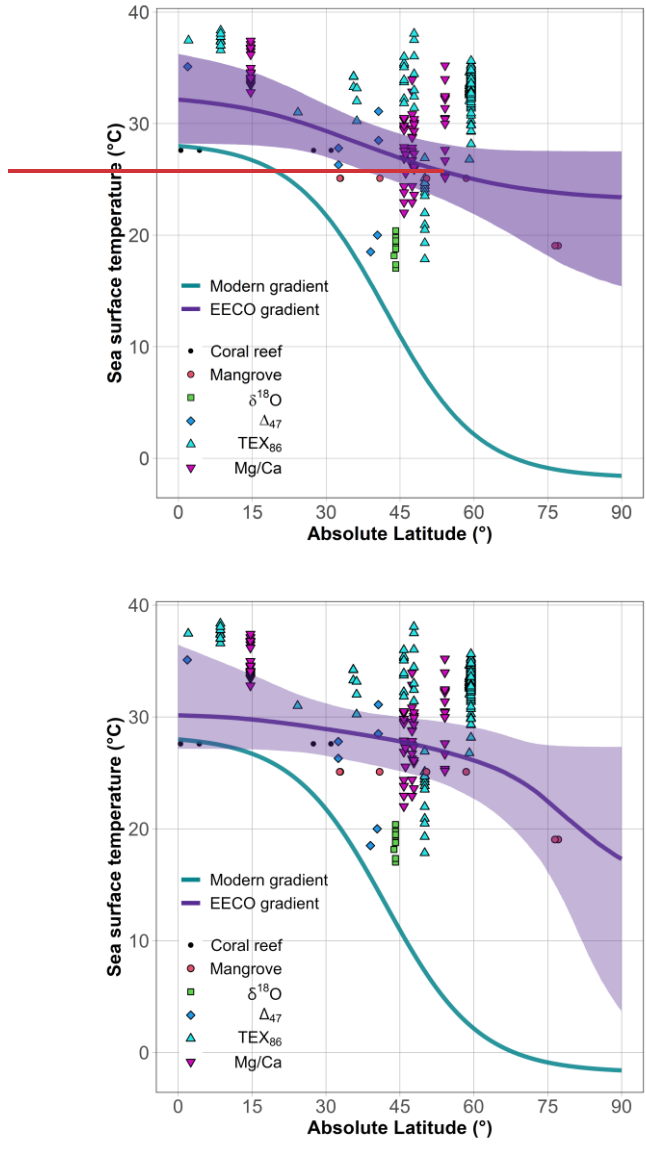


Figure 4: Estimates of the median, latitudinal sea surface temperature gradients of the early Eocene climatic optimum (purple line) and of the present-day (turquoise), both estimated with the Bayesian model. The purple ribbon (shading) depicts the 95% credible interval of the Eocene gradient, the uncertainty of the modern gradient is too low to be visible. Points within the plot depict the

geochemical (e.g. TEX₈₆) and the ecological (e.g. mangroves) data. Geochemical data are plotted by their point estimate temperature value. Ecological data are plotted at the mean temperature values of their respective normal distributions.

364 Discussion

365 Improved estimation of latitudinal and global palaeotemperatures

366 Our results show that our Bayesian model can be used to reconstruct different types of latitudinal SST
367 gradients from proxy data—~~even~~ with ~~small~~moderate sample sizes ($n = 10$ —~~20~~—34) and patchy sampling
368 distributions (Fig. 2). This is an advancement over previously used linear, quadratic, or Gaussian
369 approximations (e.g. Bijl et al., 2009; Tierney et al., 2017), which can fit only specific types of gradients.
370 As such, our model presents an alternative to non-parametric methods for inferring latitudinal temperature
371 gradients, which are sometimes favoured as they can flexibly follow the shape of an unknown temperature
372 gradient (e.g. Zhang et al., 2019; Jones and Eichenseer, 2022). However, when used for interpolation or
373 prediction outside the proxy range, non-parametric methods such as Gaussian process regression strictly
374 respond to the data (e.g. Inglis et al., 2020). This means that the idiosyncrasies of a patchy proxy record,
375 potentially afflicted with measurement errors, calibration errors, and palaeogeographic and temporal
376 uncertainty; (e.g. Buffan et al., 2023), dictate the reconstruction of large-scale ~~climate~~climatic patterns,
377 without the option of including additional knowledge (e.g. that latitudinal temperature gradients should be
378 broadly negative).

379 In contrast, our Bayesian parametric model allows for the inclusion of informative priors on the model
380 parameters. The modelled sea surface temperature gradient thus does not strictly follow the proxy data, but
381 instead represents a compromise between the data and prior knowledge. In the EECO example (Fig. 4), the
382 inclusion of informative priors improves the prediction of sea surface temperatures in the unsampled, very
383 high latitudes: Notice that the upper limit of the credible interval does not increase beyond the range of the
384 data, whereas unconstrained approaches such as splines, Gaussian processes or even standard linear
385 regression could lead to unrealistically high upper bounds in this case (see Rasmussen and Williams, 2004).
386 Prior information on the shape of latitudinal temperature gradients on Earth exists for all geological time
387 periods. For example, the greater amount of solar radiation per unit area in low latitudes causes Earth's
388 latitudinal temperature gradient to be broadly negative (Beer et al., 2008). The ease with which such prior
389 information can be integrated is a major advantage of our method, as the shape of the modelled gradient is
390 controlled by four parameters which clearly relate to its magnitude, steepness, and the latitude of its greatest
391 steepness.

392 Palaeoclimate reconstructions are often summarised as global mean surface temperatures (GMST),
393 providing a standardised metric for characterising the state of the Earth’s climate (Royer et al., 2004; Inglis
394 et al., 2020). The calculation of global mean surface temperatures directly from sparse proxy data is
395 susceptible to bias (Jones and Eichenseer, 2022). By modelling the temperature variation across latitudes,
396 a complete temperature distribution along a latitudinal axis can be obtained, filling in gaps in the proxy
397 record through inter- or extrapolation. This eliminates the common problem that specific climateclimatic
398 zones dominate the proxy record. Reconstructing the GMST directly from the proxies would lead to an
399 estimate biased towards the well-sampled latitudes. Calculating zonal averages alleviates this problem, but
400 this method relies on comprehensive latitudinal coverage (Inglis et al., 2020). Instead, our method allows
401 for intersecting the modelled temperature gradient at narrow latitudinal intervals, even when significant
402 latitudinal gaps exist. Weighting the temperatures of those latitudinal intervals by area results in GMST
403 estimates without intrinsic spatial biases. We anticipate that this improved method may significantly alter
404 Phanerozoic, proxy-based temperature curves, which have often been directly calculated from the proxy
405 record (Royer et al., 2004; Veizer and Prokoph, 2015). This is particularly relevant for the early Mesozoic
406 and older intervals, for which the spatial coverage is generally poor due to the absence of data from ocean
407 drilling sites (Jones and Eichenseer, 2022).

408 **The role of ecological constraints in palaeoclimatepalaeoclimatic** 409 **reconstructions**

410 Our results further exemplify how incorporating quantified ecological temperature constraints can provide
411 more precise temperature reconstructions than geochemical proxies alone, adding to the advances in
412 palaeoclimatepalaeoclimatic reconstructions achieved by integrating lithological data (Scotese et al., 2021;
413 Burgener et al., 2023). Combining the occurrences of climate-sensitive plant communities (Greenwood and
414 Wing, 1995), reptiles (Markwick, 2007), and leaf shapes (Peppe et al., 2011), with geochemical proxies
415 offers substantial potential for improving quantitative palaeoclimatepalaeoclimatic reconstructions across
416 the Phanerozoic. Our modelling framework offers a straightforward, efficient way of integrating ecological
417 climatepalaeoclimatic data with other proxy data: The hierarchical model structure accounts for variation
418 of temperature estimates from proxies at individual localities, which is treated equivalent to the uncertainty
419 associated with the ecological temperature proxies. A local temperature estimate, based on multiple
420 geochemical proxies, thus has the same weight as a local temperature estimate obtained from the occurrence
421 of a climate-sensitive plant community, whilst preserving the uncertainty associated with each estimate.
422 The model could easily be extended to include uncertainties on individual geochemical proxy data (see Fig.
423 S5), or to variably weight proxy records classified as more or less reliable.

424 Our approach for deriving fully quantitative climate reconstructions from ecological data is borrowed from
425 nearest living relative methods, commonly employed in terrestrial, Cenozoic ~~climate~~palaeoclimatic
426 reconstructions (Fauquette et al., 2007; Pross et al., 2012). One major limitation to these methods is that the
427 thermal preferences of taxa may have changed over time. More significantly, in the early Eocene, sea
428 surface temperatures may have reached heights unknown in the modern world, and nearest living relative
429 methods based on the modern are inherently unable to predict such elevated temperatures. This is especially
430 true for taxa that inhabit the warmest part of the ocean today, e.g. coral reefs (Kleypas et al., 1999).
431 Although coral reefs are threatened by warming sea surface temperatures today (Hoegh-Guldberg, 2011),
432 it is conceivable that Eocene reef corals were adapted to a warmer climate. The fossil record indicates that
433 reef development may have been stunted in the early Eocene, with few early Eocene coral reefs occurring
434 in low latitudes (Zamagni et al., 2012). The absence of coral reefs in higher latitudes in the early Eocene
435 could be due to requirements in irradiance, rather than temperature (Muir et al., 2015). Tropical
436 temperatures predicted by the geochemical proxy record indicate hotter-than-modern tropical temperatures
437 for the early Eocene (Fig. S2), suggesting that the modern ~~climate~~climatic range of coral reefs may
438 underestimate the early Eocene thermal ~~niche~~limits for coral reefs. We have tried to account for that
439 possibility by widening the temperature probability distribution for coral reefs, but the predicted
440 temperatures for the reef and mangrove sites still lie below the temperatures indicated by the geochemical
441 proxy record (Fig. 4, Fig. S2).

442 **Early Eocene climate**

443 The geochemical proxy record and ecological data indicate that the latitudinal SST gradient of the early
444 Eocene climatic optimum was significantly shallower than the modern (Huber and Caballero, 2011), but
445 beyond that, there is little agreement. Earlier, reconstructed early Eocene and EECO SST gradients range
446 from ~~7—~~21°C (Table 1); a more recent reconstruction that includes terrestrial air and sea surface
447 temperatures arrives at a gradient of ~13°C (Inglis et al., 2020). Our ~~polar-circle-median poles-to-equatorial-~~
448 ~~equator~~ gradient estimate is ~~lower than most previous estimates~~ similar at ~~7~~13.3°C, but notably shallower
449 ~~when taking the equator-to-polar-circle estimate, 5.8°C, although the 95% credible interval extends as the~~
450 ~~geochemical proxy data suggest high temperatures~~ up to 13.7°C and thus overlaps earlier estimates based
451 ~~on shallow water proxies. The confirmation~~ latitudes of a very flat gradient by both ~60°. Both geochemical
452 and ecological shallow water data ~~indicates~~indicate that inferred SST gradients based on tropical, shallow
453 water and deep water samples (Cramwinckel et al., 2018; Evans et al., 2018) may overestimate the SST
454 gradient of the early Eocene greenhouse world. Likewise, palaeoclimatic simulations from General
455 Circulation Models tend to estimate steeper gradients than most proxy records (Table 1; Pross et al., 2012;
456 Lunt et al., 2021)

457 ~~Discrepancies between earlier, proxy-based reconstructions and our modelling results are most pronounced~~
458 ~~in latitudes beyond the polar circle, as earlier approaches (e.g. Tierney et al., 2017) predict almost linearly~~
459 ~~decreasing SSTs towards the poles, whereas our median prediction suggests only a slight decrease beyond~~
460 ~~the polar circle. The scarcity of temperature records in this range leads to widening credible intervals in our~~
461 ~~prediction, including the possibility of stronger temperature decreases. Polar temperature estimates from~~
462 ~~our model are thus conservative in that they admit large uncertainty where data is absent, which is desirable.~~
463 ~~However, the presence of high-proxy derived temperature estimates at ~60° latitudes forces the modelled~~
464 ~~median temperature curve to be too high at ~24°C, relative to the temperatures indicated by the high-~~
465 ~~latitude mangrove communities (15.6–22.5°C). In contrast, the extrapolated polar temperatures of most~~
466 ~~previous proxy-based models are likely too low, given the abundance of ecological data indicating~~
467 ~~temperate or subtropical high-latitude climates during the EECO (Pross et al., 2012; Popescu et al., 2021).~~

468 The very high variability of the proxy record in mid-latitudes results in large uncertainties on the shape of
469 temperature gradient and on the GMST. ~~Some of this variability may stem from spatial variability in SSTs,~~
470 ~~as can be observed in the modern (Fig. 3), e.g. due to ocean circulation (Rahmstorf, 2002). Biases and errors~~
471 ~~in the proxy reconstructions also likely contribute to the observed variability, as geochemical proxies reflect~~
472 ~~many other factors besides seawater temperature (Hollis et al., 2019). Despite excluding $\delta^{18}\text{O}$ measurements~~
473 ~~from recrystallised fossils, systematic offsets remain between mostly warm temperatures derived from~~
474 ~~TEX₈₆, and cooler temperatures derived from $\delta^{18}\text{O}$, Δ_{47} , and the ecological proxies. Seasonality (Keating-~~
475 ~~Bitonti et al., 2011) and temporal changes within the EECO (Westerhold et al., 2018) may also contribute~~
476 ~~to the large variability of the EECO proxy data.~~

477 ~~Temporal changes within the EECO (Westerhold et al., 2018), and seasonality (Keating-Bitonti et al., 2011;~~
478 ~~Ivany and Judd, 2022) may also contribute to the large variability of the EECO proxy data. Based on the~~
479 ~~occurrence of heterotrophic carbonates, Davies et al. (2019) suggested that mid- and high-latitude~~
480 ~~geochemical proxy data from the EECO may be biased towards summer temperatures. Some of the~~
481 ~~geochemical mid-latitude geochemical proxy data from Hollis et al. (2019) may therefore suggest higher~~
482 ~~than actual mean annual temperatures, and the variability of temperature estimates from individual localities~~
483 ~~is higher in mid- high latitudes (Fig. S6). It is difficult to attribute this variability to seasonality alone, as~~
484 ~~temporal climate variability is also expected to be higher in mid and high latitudes (Schwartz, 2008).~~
485 ~~Critically, however, the mangrove data strongly supports our inference of a flattened gradient independent~~
486 ~~of the geochemical proxy record.~~

487 Recent, marine GMST estimates of the EECO and of the early Eocene range from 23.4–37.1°C, with the
488 lowest GMSTs being derived from $\delta^{18}\text{O}$, and the higher estimates including TEX₈₆ (Inglis et al., 2020).
489 Many studies include both marine and terrestrial proxies to derive GMST estimates, but despite great

490 differences in proxy selection and in the calculation of global average temperatures, many recent estimates
491 fall in the range of 27 - 29.5°C (Hansen et al., 2013; Caballero and Huber, 2013; Cramwinckel et al., 2018;
492 Zhu et al., 2019), similar to our median GMST estimate of 28.73°C and well within the 95% credible
493 interval of our GMST estimate (26.7–3–30.3°C).

494 Conclusions

495 The Bayesian hierarchical model presented here is able to reconstruct latitudinal gradients from both
496 geochemical and ecological proxy data, while reflecting the uncertainty associated with the ecological
497 temperature proxies, and accounting for the variation of multiple temperature estimates at individual
498 localities. Using informative prior information allows for accurate temperature reconstructions from records
499 with geographically ~~incomplete~~^{sparse} sampling. By providing temperature estimates across the entire
500 latitudinal range, this method also facilitates the reconstruction of unbiased global average temperatures.
501 Application of our model to the EECO suggests that latitudinal sea surface temperature gradients were
502 shallower than estimated by most previous proxy-based studies. High-latitude pollen records support this
503 interpretation. Our GMST estimate is in good agreement with most existing estimates, indicating that
504 broadly accurate GMST reconstructions are possible even with substantial deviations in the shape of the
505 latitudinal temperature gradient. Our new method opens the door for improving the accuracy of proxy-
506 based ~~palaeoclimate~~^{palaeoclimatic} reconstructions and Phanerozoic temperature curves, particularly in
507 intervals with a patchy and ~~unenvenly~~^{unevenly} sampled record. Finally, the flexibility of our approach
508 means that estimates can be efficiently updated when new data, or constraints, are made available.

509 Acknowledgements

510 The authors are grateful to all those who have enabled this work by collecting, measuring, collating, and
511 screening geochemical and fossil data. The contribution of L.A.J. was supported by a Juan de la Cierva-
512 formación 2021 fellowship (FJC2021-046695-I/MCIN/AEI/10.13039/501100011033) from the European
513 Union “NextGenerationEU”/PRTR. For the purpose of open access, the authors have applied a Creative
514 Commons Attribution (CC BY) licence to any Author Accepted Manuscript version arising from this
515 submission.

516 **Author contributions**

517 Both authors designed the study and carried out data preparation. K.E. programmed the model and
518 conducted the analyses. L.A.J. and K.E. generated the figures. Both authors contributed to the writing of
519 the manuscript.

520 **Competing Interests**

521 The authors declare that they have no conflicts of interest.

522 **Data accessibility**

523 The data and code used to produce the results of this study are available via GitHub
524 (<https://github.com/KEichenseer/PalaeoClimateGradient>) and the linked Zenodo repository
525 (<https://zenodo.org/record/84025307995969>).

526 **References**

- 527 Assis, J., Tyberghein, L., Bosch, S., Verbruggen, H., Serrão, E. A., and De Clerck, O.: Bio-ORACLE v2.
528 0: Extending marine data layers for bioclimatic modelling, *Global Ecology and Biogeography*, 27, 277–
529 284, 2018.
- 530 Beer, J., Abreu, J., and Steinhilber, F.: Sun and planets from a climate point of view, *Proceedings of the*
531 *International Astronomical Union*, 4, 29–43, 2008.
- 532 Bijl, P. K., Schouten, S., Sluijs, A., Reichert, G.-J., Zachos, J. C., and Brinkhuis, H.: Early Palaeogene
533 temperature evolution of the southwest Pacific Ocean, *Nature*, 461, 776–779,
534 <https://doi.org/10.1038/nature08399>, 2009.
- 535 [Buffan, L., Jones, L. A., Domeier, M., Scotese, C. R., Zahirovic, S., and Varela, S.: Mind the uncertainty:
536 Global plate model choice impacts deep-time palaeobiological studies, 2023.](#)
- 537 Burgener, L., Hyland, E., Reich, B. J., and Scotese, C.: Cretaceous climates: Mapping paleo-köppen
538 climatic zones using a bayesian statistical analysis of lithologic, paleontologic, and geochemical proxies,
539 *Palaeogeography, Palaeoclimatology, Palaeoecology*, 111373, 2023.
- 540 Burke, K. D., Williams, J. W., Chandler, M. A., Haywood, A. M., Lunt, D. J., and Otto-Bliesner, B. L.:
541 Pliocene and Eocene provide best analogs for near-future climates, *Proceedings of the National Academy*
542 *of Sciences*, 115, 13288–13293, <https://doi.org/10.1073/pnas.1809600115>, 2018.
- 543 Caballero, R. and Huber, M.: State-dependent climate sensitivity in past warm climates and its
544 implications for future climate projections, *Proceedings of the National Academy of Sciences*, 110,
545 14162–14167, 2013.

546 Chandra, R., Cripps, S., Butterworth, N., and Muller, R. D.: Precipitation reconstruction from climate-
547 sensitive lithologies using Bayesian machine learning, *Environmental Modelling & Software*, 139,
548 105002, <https://doi.org/10.1016/j.envsoft.2021.105002>, 2021.

549 Cramwinckel, M. J., Huber, M., Kocken, I. J., Agnini, C., Bijl, P. K., Bohaty, S. M., Frieling, J., Goldner,
550 A., Hilgen, F. J., Kip, E. L., et al.: Synchronous tropical and polar temperature evolution in the eocene,
551 *Nature*, 559, 382–386, 2018.

552 [Davies, A., Hunter, S. J., Gréselle, B., Haywood, A. M., and Robson, C.: Evidence for seasonality in early](#)
553 [eocene high latitude sea-surface temperatures, *Earth and Planetary Science Letters*, 519, 274–283, 2019.](#)

554 Evans, D., Sagoo, N., Renema, W., Cotton, L. J., Müller, W., Todd, J. A., Saraswati, P. K., Stassen, P.,
555 Ziegler, M., Pearson, P. N., et al.: Eocene greenhouse climate revealed by coupled clumped isotope-mg/ca
556 thermometry, *Proceedings of the National Academy of Sciences*, 115, 1174–1179, 2018.

557 Fauquette, S., Suc, J., Jiménez-Moreno, G., Micheels, A., and JOSTS, A.: Latitudinal climatic gradients
558 in the western european and mediterranean regions from the mid-miocene (c. 15 ma) to the, Deep-time
559 perspectives on climate change: marrying the signal from computer models and biological proxies, 481,
560 2007.

561 Frakes, L. A., Francis, J. E., and Syktus, J. I.: *Climate modes of the phanerozoic*, 1992.

562 Gelman, A., Carlin, J. B., Stern, H. S., Dunson, D. B., Vehtari, A., and Rubin, D. B.: *Bayesian data*
563 *analysis*, CRC press, 2013.

564 Gelman, A., Goodrich, B., Gabry, J., and Vehtari, A.: R-squared for bayesian regression models, *The*
565 *American Statistician*, 2019.

566 Gilks, W. R., Richardson, S., and Spiegelhalter, D.: *Markov chain monte carlo in practice*, CRC press,
567 1995.

568 Greenwood, D., Keefe, R., Reichgelt, T., and Webb, J.: Eocene paleobotanical altimetry of victoria’s
569 eastern uplands, *Australian Journal of Earth Sciences*, 64, 625–637, 2017.

570 Greenwood, D. R. and Wing, S. L.: Eocene continental climates and latitudinal temperature gradients,
571 *Geology*, 23, 1044, [https://doi.org/10.1130/0091-7613\(1995\)023<1044:ECCALT>2.3.CO;2](https://doi.org/10.1130/0091-7613(1995)023<1044:ECCALT>2.3.CO;2), 1995.

572 Grossman, E. L. and Joachimski, M. M.: Ocean temperatures through the phanerozoic reassessed,
573 *Scientific Reports*, 12, 8938, 2022.

574 Hansen, J., Sato, M., Russell, G., and Kharecha, P.: Climate sensitivity, sea level and atmospheric carbon
575 dioxide, *Philosophical Transactions of the Royal Society A: Mathematical, Physical and Engineering*
576 *Sciences*, 371, 20120294, 2013.

577 Hoegh-Guldberg, O.: Coral reef ecosystems and anthropogenic climate change, *Regional Environmental*
578 *Change*, 11, 215–227, 2011.

579 Hollis, C. J., Dunkley Jones, T., Anagnostou, E., Bijl, P. K., Cramwinckel, M. J., Cui, Y., Dickens, G. R.,
580 Edgar, K. M., Eley, Y., Evans, D., et al.: The DeepMIP contribution to PMIP4: Methodologies for
581 selection, compilation and analysis of latest paleocene and early eocene climate proxy data, incorporating
582 version 0.1 of the DeepMIP database, *Geoscientific Model Development*, 12, 3149–3206, 2019.

583 Huber, M. and Caballero, R.: The early eocene equable climate problem revisited, *Climate of the Past*, 7,
584 603–633, 2011.

585 Inglis, G. N., Bragg, F., Burls, N. J., Cramwinckel, M. J., Evans, D., Foster, G. L., Huber, M., Lunt, D. J.,
586 Siler, N., Steinig, S., Tierney, J. E., Wilkinson, R., Anagnostou, E., de Boer, A. M., Dunkley Jones, T.,
587 Edgar, K. M., Hollis, C. J., Hutchinson, D. K., and Pancost, R. D.: Global mean surface temperature and
588 climate sensitivity of the early Eocene Climatic Optimum (EECO), Paleocene (PETM), and latest
589 Paleocene, *Climate of the Past*, 16, 1953–1968, <https://doi.org/10.5194/cp-16-1953-2020>, 2020.

590 [Ivany, L. C. and Judd, E. J.: Deciphering temperature seasonality in earth's ancient oceans, *Annual*](#)
591 [Review of Earth and Planetary Sciences](#), 50, 123–152, 2022.

592 Johannes, R., Wiebe, W., Crossland, C., Rimmer, D., and Smith, S.: Latitudinal limits of coral reef
593 growth., *Marine ecology progress series*. Oldendorf, 11, 105–111, 1983.

594 Jones, L. A. and Eichenseer, K.: Uneven spatial sampling distorts reconstructions of Phanerozoic
595 seawater temperature, *Geology*, 50, 238–242, <https://doi.org/10.1130/G49132.1>, 2022.

596 Jones, L. A., Mannion, P. D., Farnsworth, A., Bragg, F., and Lunt, D. J.: Climatic and tectonic drivers
597 shaped the tropical distribution of coral reefs, *Nature communications*, 13, 1–10, 2022.

598 Jones, L. A., Gearty, W., Allen, B. J., Eichenseer, K., Dean, C. D., Galván, S., Kouvari, M., Godoy, P. L.,
599 Nicholl, C., Buffan, L., Flannery-Sutherland, J. T., Dillon, E. M., and Chiarenza, A. A.: palaeoverse: a
600 community-driven R package to support palaeobiological analysis, <https://doi.org/10.31223/X5Z94Q>,
601 2023.

602 Judd, E. J., Bhattacharya, T., and Ivany, L. C.: A Dynamical Framework for Interpreting Ancient Sea
603 Surface Temperatures, *Geophysical Research Letters*, 47, e2020GL089044,
604 <https://doi.org/10.1029/2020GL089044>, 2020.

605 Judd, E. J., Tierney, J. E., Huber, B. T., Wing, S. L., Lunt, D. J., Ford, H. L., Inglis, G. N., McClymont,
606 E. L., O'Brien, C. L., Rattanasriampaipong, R., et al.: The PhanSST global database of phanerozoic sea
607 surface temperature proxy data, *Scientific data*, 9, 753, 2022.

608 Keating-Bitonti, C. R., Ivany, L. C., Affek, H. P., Douglas, P., and Samson, S. D.: Warm, not super-hot,
609 temperatures in the early Eocene subtropics, *Geology*, 39, 771–774, <https://doi.org/10.1130/G32054.1>,
610 2011.

611 Kiessling, W.: Paleoclimatic significance of phanerozoic reefs, *Geology*, 29, 751–754, 2001.

612 Kleypas, J. A., McManus, J. W., and Meñez, L. A.: Environmental limits to coral reef development:
613 Where do we draw the line?, *American zoologist*, 39, 146–159, 1999.

614 [Lunt, D. J., Bragg, F., Chan, W.-L., Hutchinson, D. K., Ladant, J.-B., Morozova, P., Niezgodzki, I.,](#)
615 [Steinig, S., Zhang, Z., Zhu, J., et al.: DeepMIP: Model intercomparison of early eocene climatic optimum](#)
616 [\(EECO\) large-scale climate features and comparison with proxy data, *Climate of the Past*, 17, 203–227,](#)
617 [2021.](#)

618 Markwick, P.: The palaeogeographic and palaeoclimatic significance of climate, Deep-time perspectives
619 on climate change: Marrying the signal from computer models and biological proxies, 251, 2007.

620 Markwick, P. J.: "Equability," continentality, and tertiary "climate": The crocodylian perspective,
621 *Geology*, 22, 613–616, 1994.

622 [McElreath, R.: Statistical rethinking: A bayesian course with examples in r and stan, Chapman:](#)
623 [Hall/CRC, 2018.](#)

624 Merdith, A. S., Williams, S. E., Collins, A. S., Tetley, M. G., Mulder, J. A., Blades, M. L., Young, A.,
625 Armistead, S. E., Cannon, J., Zahirovic, S., et al.: Extending full-plate tectonic models into deep time:
626 Linking the neoproterozoic and the phanerozoic, *Earth-Science Reviews*, 214, 103477, 2021.

627 Muir, P. R., Wallace, C. C., Done, T., and Aguirre, J. D.: Limited scope for latitudinal extension of reef
628 corals, *Science*, 348, 1135–1138, 2015.

629 Peppe, D. J., Royer, D. L., Cariglino, B., Oliver, S. Y., Newman, S., Leight, E., Enikolopov, G.,
630 Fernandez-Burgos, M., Herrera, F., Adams, J. M., et al.: Sensitivity of leaf size and shape to climate:
631 Global patterns and paleoclimatic applications, *New phytologist*, 190, 724–739, 2011.

632 Popescu, S.-M., Suc, J.-P., Fauquette, S., Bessedik, M., Jiménez-Moreno, G., Robin, C., and Labrousse,
633 L.: Mangrove distribution and diversity during three Cenozoic thermal maxima in the Northern
634 Hemisphere (pollen records from the Arctic regions), *Journal of Biogeography*, 48, 2771–2784,
635 <https://doi.org/10.1111/jbi.14238>, 2021.

636 Pross, J., Contreras, L., Bijl, P. K., Greenwood, D. R., Bohaty, S. M., Schouten, S., Bendle, J. A., Röhl,
637 U., Tauxe, L., Raine, J. I., Huck, C. E., van de Flierdt, T., Jamieson, S. S. R., Stickley, C. E., van de
638 Schootbrugge, B., Escutia, C., and Brinkhuis, H.: Persistent near-tropical warmth on the Antarctic
639 continent during the early Eocene epoch, *Nature*, 488, 73–77, <https://doi.org/10.1038/nature11300>, 2012.

640 Quisthoudt, K., Schmitz, N., Randin, C. F., Dahdouh-Guebas, F., Robert, E. M. R., and Koedam, N.:
641 Temperature variation among mangrove latitudinal range limits worldwide, *Trees*, 26, 1919–1931,
642 <https://doi.org/10.1007/s00468-012-0760-1>, 2012.

643 [Rahmstorf, S.: Ocean circulation and climate during the past 120,000 years, *Nature*, 419, 207–214, 2002.](#)

644 Rasmussen, C. E. and Williams, C. K.: Gaussian processes in machine learning, *Lecture notes in*
645 *computer science*, 3176, 63–71, 2004.

646 Reynolds, R. W. and Smith, T. M.: Improved global sea surface temperature analyses using optimum
647 interpolation, *Journal of climate*, 7, 929–948, 1994.

648 Royer, D. L.: Climate reconstruction from leaf size and shape: New developments and challenges, *The*
649 *Paleontological Society Papers*, 18, 195–212, 2012.

650 Royer, D. L., Berner, R. A., Montañez, I. P., Tabor, N. J., Beerling, D. J., et al.: Co₂ as a primary driver
651 of phanerozoic climate, *GSA today*, 14, 4–10, 2004.

652 Salonen, J. S., Korpela, M., Williams, J. W., and Luoto, M.: Machine-learning based reconstructions of
653 primary and secondary climate variables from north american and european fossil pollen data, *Scientific*
654 *reports*, 9, 15805, 2019.

655 Schrag, D. P.: Effects of diagenesis on the isotopic record of late paleogene tropical sea surface
656 temperatures, *Chemical Geology*, 161, 215–224, 1999.

657 [Schwartz, S. E.: Uncertainty in climate sensitivity: Causes, consequences, challenges, *Energy &*](#)
658 [environmental science](#), 1, 430–453, 2008.

659 Scotese, C. R., Song, H., Mills, B. J. W., and van der Meer, D. G.: Phanerozoic paleotemperatures: The
660 earth's changing climate during the last 540 million years, *Earth-Science Reviews*, 215, 103503,
661 <https://doi.org/10.1016/j.earscirev.2021.103503>, 2021.

662 Sloan, L. C. and Barron, E. J.: "equable" climates during earth history?, *Geology*, 18, 489–492, 1990.

- 663 Song, H., Wignall, P. B., Song, H., Dai, X., and Chu, D.: Seawater Temperature and Dissolved Oxygen
664 over the Past 500 Million Years, *Journal of Earth Science*, 30, 236–243, [https://doi.org/10.1007/s12583-](https://doi.org/10.1007/s12583-018-1002-2)
665 018-1002-2, 2019.
- 666 Suan, G., Popescu, S.-M., Suc, J.-P., Schnyder, J., Fauquette, S., Baudin, F., Yoon, D., Piepjohn, K.,
667 Sobolev, N. N., and Labrousse, L.: Subtropical climate conditions and mangrove growth in Arctic Siberia
668 during the early Eocene, *Geology*, 45, 539–542, <https://doi.org/10.1130/G38547.1>, 2017.
- 669 Taylor, S. P., Haywood, A. M., Valdes, P. J., and Sellwood, B. W.: An evaluation of two spatial
670 interpolation techniques in global sea-surface temperature reconstructions: Last Glacial Maximum and
671 Pliocene case studies, *Quaternary Science Reviews*, 23, 1041–1051,
672 <https://doi.org/10.1016/j.quascirev.2003.12.003>, 2004.
- 673 Tierney, J. E., Sinninghe Damsté, J. S., Pancost, R. D., Sluijs, A., and Zachos, J. C.: Eocene temperature
674 gradients, *Nature Geoscience*, 10, 538–539, 2017.
- 675 Tierney, J. E., Poulsen, C. J., Montañez, I. P., Bhattacharya, T., Feng, R., Ford, H. L., Hönisch, B., Inglis,
676 G. N., Petersen, S. V., Sagoo, N., et al.: Past climates inform our future, *Science*, 370, eaay3701, 2020.
- 677 Veizer, J. and Prokoph, A.: Temperatures and oxygen isotopic composition of Phanerozoic oceans, *Earth-*
678 *Science Reviews*, 146, 92–104, <https://doi.org/10.1016/j.earscirev.2015.03.008>, 2015.
- 679 Vickers, M. L., Bernasconi, S. M., Ullmann, C. V., Lode, S., Looser, N., Morales, L. G., Price, G. D.,
680 Wilby, P. R., Hougård, I. W., Hesselbo, S. P., et al.: Marine temperatures underestimated for past
681 greenhouse climate, *Scientific reports*, 11, 1–9, 2021.
- 682 [Weitzel, N., Hense, A., and Ohlwein, C.: Combining a pollen and macrofossil synthesis with climate](#)
683 [simulations for spatial reconstructions of european climate using bayesian filtering, *Climate of the Past*,](#)
684 [15, 1275–1301, 2019.](#)
- 685 Westerhold, T., Röhl, U., Donner, B., and Zachos, J. C.: Global extent of early eocene hyperthermal
686 events: A new pacific benthic foraminiferal isotope record from shatsky rise (ODP site 1209),
687 *Paleoceanography and Paleoclimatology*, 33, 626–642, 2018.
- 688 Yamano, H., Hori, K., Yamauchi, M., Yamagawa, O., and Ohmura, A.: Highest-latitude coral reef at iki
689 island, japan, *Coral Reefs*, 20, 9–12, 2001.
- 690 [Yang, D. and Bowen, G. J.: Integrating plant wax abundance and isotopes for paleo-vegetation and](#)
691 [paleoclimate reconstructions: A multi-source mixing model using a bayesian framework, *Climate of the*](#)
692 [Past, 18, 2181–2210, 2022.](#)
- 693 Zamagni, J., Mutti, M., and Košir, A.: The evolution of mid paleocene-early eocene coral communities:
694 How to survive during rapid global warming, *Palaeogeography, palaeoclimatology, palaeoecology*, 317,
695 48–65, 2012.
- 696 Zhang, L., Hay, W. W., Wang, C., and Gu, X.: The evolution of latitudinal temperature gradients from the
697 latest Cretaceous through the Present, *Earth-Science Reviews*, 189, 147–158,
698 <https://doi.org/10.1016/j.earscirev.2019.01.025>, 2019.
- 699 Zhu, J., Poulsen, C. J., and Tierney, J. E.: Simulation of eocene extreme warmth and high climate
700 sensitivity through cloud feedbacks, *Science advances*, 5, eaax1874, 2019.
- 701 Ziegler, A., Hulver, M., Lottes, A., and Schmachtenberg, W.: Uniformitarianism and palaeoclimates:
702 Inferences from the distribution of carbonate rocks, *Geological journal. Special issue*, 3–25, 1984.